Poisson ratio and bulk lattice constant of (Sr 0.25 La 0.75)CrO 3 from strained epitaxial thin films

Dong Han, Mohamed Bouras, Claude Botella, Aziz Benamrouche, Bruno Canut, Geneviève Grenet, Guillaume Saint-Girons, Romain Bachelet

Poisson ratio and bulk lattice constant of $(Sr_{0.25}La_{0.75})CrO_3$ from strained epitaxial thin films

Dong Han[1], Mohamed Bouras[1], Claude Botella[1], Aziz Benamrouche[1], Bruno Canut[2], Geneviève Grenet[1], Guillaume Saint-Girons[1], and Romain Bachelet[1,a)]

[1] *Institut des Nanotechnologies de Lyon – INL CNRS UMR 5270, Université de Lyon, Ecole Centrale de Lyon, 36 avenue Guy de Collongue, 69134 Ecully, France*

[2] *Institut des Nanotechnologies de Lyon – INL CNRS UMR 5270, Université de Lyon, INSA Lyon, 7 avenue Jean Capelle, 69621 Villeurbanne, France*

[a)] Email: romain.bachelet@ec-lyon.fr

Abstract

About 30 nm thick (001)-oriented $(Sr_{0.25}La_{0.75})CrO_3$ (SLCO) epitaxial thin films were grown by solid-source oxide molecular beam epitaxy on four different single-crystalline cubic or pseudo-cubic (001)-oriented oxide substrates: $LaAlO_3$, $(LaAlO_3)_{0.3}(Sr_2AlTaO_6)_{0.7}$, $SrTiO_3$ and $DyScO_3$, which result in lattice mismatch ranging from –2% to +1.7%. All the films are of high-quality, flat and strained by the substrates. By assessing the evolution of the out-of-plane lattice parameter as a function of the in-plane lattice parameter of the samples, we determine both the Poisson ratio (ν = 0.32) and the bulk lattice constant (a_b = 3.876 Å) of SLCO. The Poisson ratio significantly differs from $LaCrO_3$ (ν = 0.23) and the $(Sr_xLa_{1-x})CrO_3$ solid solution appears to obey structural Vegard's law. Since SLCO is the only one *p*-type transparent conductive oxide of perovskite structure and has promising thermoelectric properties, integrating SLCO in heterostructures and devices is therefore of paramount importance, which confers on our results their strong interest. Besides, the method used here can be straightforwardly applied to other complex oxides.

Key words: Poisson ratio, Bulk lattice constant, $(Sr_xLa_{1-x})CrO_3$ solid solution, Epitaxial films, Strain effect

I. INTRODUCTION

Lanthanum chromite, $LaCrO_3$ (LCO), has attracted strong attention and motivated an increasing number of studies in the past few years due to its remarkable physical properties. LCO is an antiferromagnetic insulator at room temperature[1,2] and becomes a *p*-type transparent conductor with partial substitution with divalent Sr on A-site for instance[3,4,5,6]. These tunable physical properties, enabled by the chemical flexibility characteristic for perovskite oxides, are liable to deserve many key applications and devices such as solid-oxide fuel cells (SOFC)[7], transparent electrode, thermoelectricity[5], water-splitting[8], and non-volatile memories[9,10]. LCO can also be combined by epitaxy to the other members of the perovskite oxide family, the wide ranging physical properties of which (*n*-type semiconductor[11], ferroelectric, piezoelectric,…) leverage the design of original functionalities and devices. Whereas *n*-type perovskite-oxide semiconductors, such as the widely studied $(La_xSr_{1-x})TiO_3$ and more recently $(La_xBa_{1-x})SnO_3$, are well known, $(Sr_xLa_{1-x})CrO_3$ is almost the only example of *p*-type perovskite-oxide semiconductor reported to date[12,13]. Its structural and elastic properties, whilst crucial to control the growth and properties of this material, are very poorly known[6,14].

For isotropic solids subjected to uniaxial stress, the Poisson ratio (ν) is defined as $-\varepsilon_t/\varepsilon_l$, where ε_t and ε_l are the strain in the transverse and longitudinal direction with respect to the stress direction, respectively[15]. For all isotropic materials $-1 \leq \nu \leq 0.5$, and for most well-known solids $0.2 \leq \nu \leq 0.4$[15,16]. For single-crystalline materials, a strong elastic anisotropy can exist yielding abnormal Poisson ratios[17,18]. For solids of cubic symmetry, the Poisson ratio can also be written as a function of the elastic constants as follows: $\nu = C_{12} / (C_{11} + C_{12})$. When subjected to biaxial stress, as it is the case for epitaxial films of materials with pseudo-cubic lattice (*e.g.* perovskite oxides), the normal strain (ε_{zz}, perpendicular to the plane) can be written as function of the Poisson ratio and in-plane strain along the <100> directions (ε_{xx} or ε_{yy}) as following equation[19]:

$$\varepsilon_{zz} = -\frac{2v}{1-v}\varepsilon_{xx} \quad (1)$$

Where $v / (1 - v) = C_{12}/C_{11}$. From this relationship, both the Poisson ratio and the bulk lattice constant (a_b) can be extracted by measuring the out-of-plane (c) and in-plane (a) lattice parameters of films subjected to different biaxial epitaxial strains, using the following linear relationship:

$$c = -\frac{2v}{1-v}a + \frac{1+v}{1-v}a_b \quad (2)$$

Although various studies have dealt with strain-dependent physical properties from films subjected to different strains, the extraction of Poisson ratio and bulk lattice constant is mostly absent. Only a few previous studies report the extraction of v from strained epitaxial perovskite oxide thin films. Chen *et al*.[20] have grown multiferroic $BiFeO_3$ thin films on different substrates chosen to provide the widest possible range of lattice mismatch (from –2.8% to +6%) and have measured a v value of 0.49 for the rhombohedral-like phase of this oxide. Adamo *et al*.[21] derived a Poisson ratio of 0.37 for epitaxial $La_{0.7}Sr_{0.3}MnO_3$ thin film. Choi *et al*.[22] have grown $(La_xSr_{1-x})TiO_3$ films with different substitution ratios (from 5% to 25%) on different substrates resulting in lattice mismatch strain ranging from –2.9% to +1.1%, and although the measured Poisson ratio is not given, the study indicates that Sr substitution by La tends to decrease the Poisson ratio with respect to $SrTiO_3$. Niu *et al*.[23] have evidenced the formation of two $SrTiO_3$ phases having different Poisson ratios during the epitaxial growth of this oxide on Si.

In this paper, high-quality strained epitaxial $(Sr_{0.25}La_{0.75})CrO_3$ (SLCO) and $LaCrO_3$ (LCO) thin films were grown by molecular beam epitaxy (MBE) on four different (001)-oriented (pseudo-)cubic perovskite-oxide substrates: $LaAlO_3$ (LAO), $(LaAlO_3)_{0.3}(Sr_2AlTaO_6)_{0.7}$ (LSAT), $SrTiO_3$ (STO) and $DyScO_3$ (DSO), with different lattice constants ranging from 3.796 to 3.944 Å (Fig. 1). The impact of epitaxial strain on the in- and out-of-plane lattice parameters of the thin layers has been investigated, and the Poisson ratio as

well as the bulk lattice constant of SLCO has been extracted from these measurements. The parameters significantly differ from that measured for LCO (see supplementary material).

II. EXPERIMENTAL DETAILS

Four different (001)-oriented cubic/pseudocubic perovskite-oxide substrates, namely LAO, LSAT, STO and DSO with lattice constants of 3.796 Å, 3.868 Å, 3.905 Å and 3.944 Å, respectively[24], were used to grow in the same campaign (but different runs) the strained epitaxial SLCO (~30 nm) and LCO (~15 nm) thin films by solid-source MBE in a ultra-high vacuum (UHV) chamber having a base pressure less than 1×10^{-9} Torr. La, Sr and Cr were evaporated from effusion cells in codeposition. The fluxes were measured before the growth using a Bayard-Alpert (BA) gauge (after subtraction of the background pressure) and checked using a quartz crystal microbalance (Fig. S1)[25]. The stoichiometry has been calibrated using flux measurements by BA gauge and quartz crystal microbalance (QCM), X-ray diffraction (XRD) on calibration series (LCO and $SrCrO_3$), Rutherford backscattering spectrometry (RBS) and X-ray photoelectron spectroscopy (XPS) (see Fig. S2-4). The growth rate was ~ 0.15 nm/min for the SLCO films and ~ 0.1 nm/min for LCO films. The substrates were annealed under the growth conditions for 15 minutes in order to remove surface impurities before starting the growth at T = 750°C and $P(O_2) = 1\times10^{-7}$ Torr[25]. After deposition, the substrate temperature was lowered to 200°C at a rate of 50 °C/min while the background O_2 was pumping out. All the films were grown on as-received substrates, except that grown on STO, for which the substrate was treated to be terminated by a TiO_2 plane[25,26]. Reflection high-energy electron diffraction (RHEED) was used to check *in-situ* the qualitative structural quality of the films. The structural properties were quantitatively investigated by XRD and X-ray reflectometry (XRR) using a Rigaku Smartlab diffractometer equipped with a high-brilliance rotating anode

and a double-crystal Ge(220) monochromator. Atomic force microscopy (AFM) was used to measure the surface morphology and local surface roughness of the films.

III. RESULTS AND DISCUSSION

The RHEED patterns recorded at the end of the growth of the SLCO thin films on the four different substrates along the high-symmetry <100> in-plane crystallographic direction are shown in Fig. 2a-d. All the patterns, except that corresponding to the film grown on the LAO substrate (Fig. 2a), present well contrasted streak lines showing that the films are heteroepitaxial with very flat surfaces. For the film grown on LAO, the rather spotty pattern indicates that the film is slightly rougher than the others. Indeed, according to XRR measurements, the SLCO/LAO film surface has a mean root-mean-square (rms) roughness around 0.72 nm that is slightly larger than that of the three other SLCO films on LSAT, STO, and DSO substrates, which are 0.58 nm, 0.54 nm and 0.49 nm, respectively. Besides, the rms substrate surface roughness is found to be very low (0.15 nm) for all the cases (Table S2). The rms surface roughnesses measured locally by AFM topographic images are in good agreement with RHEED and XRR results (Fig. S6).

The structural properties of all SLCO and LCO films have been investigated by XRD. Wide 2θ-ω scans (10-80°) reveal only diffraction peaks corresponding to the {00l} reflections of the SLCO films and substrates (Fig. S7), indicating that no other (001) oriented phases than SLCO (00l) are present in the epitaxial films. In addition, XRD pole figure performed on the SLCO film on LAO (the largest lattice mismatch) does not reveal any secondary crystalline phase (Fig. S8). Fig. 2e-h show the XRD 2θ-ω scans around the (002) reflections of SLCO films and their corresponding substrates. The presence of Pendellosung fringes around the diffraction peaks of films attest their high crystalline quality and abrupt interfaces. The out-of-plane lattice parameter of the SLCO films (c_{SLCO}) decreases with increasing substrate lattice

constant, due to increasing in-plane strain. The same behavior is observed for LCO films (Fig. S11b), which is ruled by elasticity Hooke's law with positive Poisson ratio[19]. The c_{SLCO} values are 3.943 Å, 3.904 Å, 3.844 Å, and 3.804 Å for SLCO films on LAO, LSAT, STO and DSO substrates, respectively. Although the films are of similar thickness (Table S2, Table 1), the (002) peaks of SLCO films on LAO and DSO are wider than those of SLCO films on LSAT and STO with lower lattice mismatch, indicating a wider distribution of out-of-plane lattice parameter. Most probably, a beginning of strain relaxation occurs at this thickness with such large lattice mismatch. For the SLCO film on DSO, two secondary maxima seem to be visible, indicating the presence of two main out-of-plane parameters (3.795 Å and 3.815 Å), but both being much lower than the expected/measured bulk value (3.876 Å, see below). A single fit with a main component leads to an out-of-plane parameter of 3.804 Å (Fig. 2h) in perfect agreement within the instrumental resolution with the maximum of the (103) node in the reciprocal space map (Fig. 3d) corresponding to fully strained component.

Table 1: Summary of the structural and chemical properties of the SLCO thin films.

Substrate	Lattice mismatch (%)	Thickness (nm)	[A/(A+B)] (at%)	[Sr] (at%)	*a* (Å)	*c* (Å)	Mosaicity (°)	Substrate roughness (nm)	Film roughness (nm)
LAO	-2.06	27.2	49.8	23.8	3.796	3.943	0.38	0.15	0.72
LSAT	-0.21	29.9	56.2	24.8	3.868	3.904	0.07	0.15	0.58
STO	0.75	29.2	54.5	24.5	3.905	3.844	0.08	0.15	0.54
DSO	1.75	29.0	52.9	26.0	3.944	3.804	0.09	0.15	0.49

The ω-scans measured for all the films around the SLCO (002) reflection are shown in Fig. 2i. The mosaicity (full width at half maximum, FWHM, of these curves) is below 0.09° for all films except for SLCO on LAO, indicating high structural quality. For the SLCO film grown on LAO substrate, the mosaicity is larger around 0.38°, probably partially because of the poor crystalline quality of the substrate, large in-plane compressive stress and partial plastic relaxation with 3D morphology (Fig. 2a). Fig. 2j shows the normalized integrated diffracted

intensity of these ω-scans as a function of the substrate lattice constant. The highest intensity is obtained for the smallest lattice mismatch, showing the impact of epitaxial strain on the structural quality.

The in-plane parameters of the SLCO and LCO thin films have been measured using XRD reciprocal space maps (RSM) around the asymmetrical (103) reflections (Fig. 3 and Fig. S10, respectively). These RSM besides confirm the tendencies extracted from Fig. 2e-h (and Fig. S9e-h) for the out-of-plane lattice parameter. For the DSO, STO and LSAT substrates, the SLCO (103) nodes are aligned vertically with that of the substrates, indicating that the in-plane lattice parameter of the SLCO thin films (a_{SLCO}) are equal to that of their substrates, and thus that the films are coherently strained by the substrates. For the SLCO film on LAO substrate, the node asymmetry attest for partial strain relaxation, which is most probably due to a larger lattice mismatch on this substrate (see below)[27]. The same main behavior is observed with the LCO epitaxial thin films (Fig. S10). However, looking into more details, the (103) nodes of the SLCO films on LAO and DSO are both asymmetric, with broadening elongated towards a slightly different position than the bulk position (Fig. 3). Although low, thermal expansion mismatch between the film and substrates can mitigate this discrepancy, as in the case of LCO films (Fig. S10)[28,29]. The remaining difference could be caused by slight cationic segregations, as observed with other Cr-based oxides but with spinel structure[30]. In the following, the Poisson ratio and bulk lattice constant of SLCO and LCO are derived from the fully strained part of the films.

The dependence of the out-of-plane lattice parameters c to the in-plane lattice parameter a is shown for both SLCO and LCO films in Fig. 4. The $c(a)$ function is linear as expected from elastic strain of pseudo-cubic SLCO[19], and it can be fitted using Eq. (2). The Poisson ratio (ν =

0.32 ± 0.02) as well as the bulk lattice constant (a_b = 3.876 Å) and $C_{12}/C_{11} = \nu / (1 - \nu) \sim 0.5$ of SLCO have been extracted from such fit. Note that this method applied to LCO (Fig. S11b) leads to elastic and structural parameters very similar to those found in the literature, confirming its validity: the measured Poisson ratio (ν = 0.24) and bulk lattice constant (a_b = 3.888 Å) are in perfect agreement with literature (ν = 0.23 and a_b = 3.885 Å)[14,31]. The 25% Sr substitution significantly increases the Poisson ratio by more than 30% with respect to LCO. The change of Poisson ratio might also be related to the change in Cr valence rather than the Sr substitution alone. In order to well discriminate the cause, other SLCO films with lower oxidation state would have to be elaborated in order to get the same Cr valence as in LCO films. The inset of Fig. 4 indicates that the bulk lattice constant of SLCO ($a_{b\text{-SLCO}}$ = 3.876 Å) is linearly in-between that of LCO ($a_{b\text{-LCO}}$ = 3.885 Å)[31] and $SrCrO_3$ (SCO) ($a_{b\text{-SCO}}$ = 3.819 Å)[13,32], which is expected from a Vegard's law and is in agreement with literature[6]. The bulk lattice constant of SLCO is thus in-between of that of LSAT and STO substrates (closer to LSAT whose lattice constant is 3.868 Å) and confirms that the SLCO film with the lowest strain is the one grown on LSAT substrate.

Fig. 5 shows a summary of the structural properties (lattice parameters and associated strains) of the epitaxial SLCO films as a function of the substrate lattice constants and the structural mismatch (f_0). The out-of-plane strain (ε_{zz}) is inversely equal to the in-plane strain (ε_{xx}), consistently with the measured Poisson ratio value (Fig. 5a-b). For $\nu = 1/3$, $\varepsilon_{zz} = -\varepsilon_{xx}$ [Eq. (1)]. The SLCO epitaxial thin films can endure relatively large strain up to 2% and can present relatively large (pseudo)tetragonality (c/a) almost up to 1.05 (Fig. 5c), much more important than bulk tetragonal ferroelectric $BaTiO_3$ (c/a = 1.01) for instance. The unit-cell volume is found to be in-between 57 and 59 Å^3 ($V_{b\text{-SLCO}}$ = 58.231 Å^3) and the relative volume change within the 2% range (Fig. 5d), in agreement with this Poisson ratio value. Film density is around

6.45 g cm^{-3} for all films consistently with the bulk density. Epitaxial strain of SLCO films having relatively large Poisson ratio could have a great impact on their physical properties which is barely unexplored to date.

IV. CONCLUSION

In summary, high-quality epitaxial thin films of $(Sr_{0.25}La_{0.75})CrO_3$ (SLCO) solid solutions as well as $LaCrO_3$ (LCO) were grown by MBE on four different (001)-oriented cubic/pseudocubic perovskite-oxide substrates: LAO, LSAT, STO and DSO, resulting in different compressive and tensile strains (from -2.06% to +1.75%). All the films crystallize in the perovskite structure, are fully (001)-oriented, flat and epitaxially strained. The out-of-plane lattice parameters of SLCO films widely vary from 3.943 Å to 3.804 Å. Both the Poisson ratio and the bulk lattice constant of SLCO have been extracted from these measurements (ν = 0.32 and a_b = 3.876 Å), which significantly differ from that of LCO. The $(Sr_xLa_{1-x})CrO_3$ solid solution appears to obey structural Vegard's law and the relatively large Poisson ratio of SLCO would enable flexible tuning of its physical properties by elastic epitaxial strain. Besides, the method used here can be straightforwardly applied to other complex oxides.

SUPPLEMENTARY MATERIAL

See supplementary material for detailed description and analysis of the MBE flux, XRD, RBS, XPS, XRR results, AFM topography of SLCO films, as well as RHEED patterns, extraction of Poisson ratio and bulk lattice constant, and summary of structural properties of LCO films.

ACKNOWLEDGMENTS

Financial support from the European Commission through the project TIPS (grant reference H2020-ICT-02-2014-1-644453) and the French research national agency (ANR) through the project MITO (grant reference No. ANR-17-CE05-0018) is acknowledged. The China Scholarship Council (CSC) is acknowledged for the grant of D. Han. The authors are also grateful to A. Danescu and P. Bonté for discussions on Poisson ratio, P. Regreny and J. B. Goure for technical support.

FIGURES AND TABLE CAPTIONS

FIG. 1: Bulk lattice constants of the films and substrates involved in the study.

FIG. 2. (a-d) RHEED patterns recorded along the <100> azimuth (around 200°C, $P(O_2) = 1\times10^{-9}$ Torr) after the growth of SLCO films on (a) LAO, (b) LSAT, (c) STO and (d) DSO substrates. (e-h) XRD 2θ-ω scans near the (002) Bragg reflections on SLCO films grown on (e) LAO, (f) LSAT, (g) STO and (h) DSO substrates with corresponding fitting curves. (i) Normalized XRD ω-scans around the SLCO (002) reflection for all films. (j) Mosaicity values as a function of the substrate used.

FIG. 3. Reciprocal space maps recorded around the asymmetric (103) reflections of SLCO thin films on (a) LAO, (b) LSAT, (c) STO and (d) DSO substrates. The vertical red dotted line and the crosses indicate respectively the Q_{xx} and Q_{zz} positions of bulk SLCO extracted in this work.

FIG. 4. Evolution of c (out-of-plane lattice parameter) as a function of a (in-plane lattice parameter) for both SLCO (violet squares) and LCO (orange triangles) epitaxial films on the four different substrates. The dotted lines represent the fits in both cases. The black square and triangle represent the bulk lattice constants of both SLCO and LCO derived from these fits. Inset indicates the variation of $Sr_xLa_{1-x}CrO_3$ bulk lattice constant (a_b) as a function of the substitution ratio (x).

FIG. 5. Summary of the structural properties of SLCO films as a function of lattice constant of the used substrates and the structural mismatch (f_0). (a) Out-of-plane lattice parameter c and out-of-plane strain ε_{zz}. (b) In-plane lattice parameter a and in-plane strain ε_{xx}. (c) The (pseudo)tetragonality c/a. (d) The unit-cell volume and the relative volume change ($\Delta V/V$).

Table 1: Summary of the structural and chemical properties of the SLCO thin films.

REFERENCES

[1]I. Weinberg and P. Larssen, Electron paramagnetic resonance and antiferromagnetism in $LaCrO_3$, Nature, **192**, 445 (1961).

[2]T. Arima, Y. Tokura, and J. B. Torrance, Variation of optical gaps in perovskite-type 3d transition-metal oxides, Phys. Rev. B **48**, 17006 (1993).

[3]J. B. Webb, M. Sayer, A. Mansingh. Polaronic conduction in lanthanum strontium chromite, Can. J. Phys. **55**, 1725 (1977).

[4]D. P. Karim and A. T. Aldred, Localized level hopping transport in $La(Sr)CrO_3$, Phys. Rev. B **20**, 2255 (1979).

[5]K. H. L. Zhang, Y. Du, A. Papadogianni, O. Bierwagen, S. Sallis, L. F. J. Piper, M. E. Bowden, V. Shutthanandan, P. V. Sushko, and S. A. Chambers, Perovskite Sr-doped $LaCrO_3$ as a new p-type transparent conducting oxide, Adv. Mater. **27**, 5191 (2015).

[6]K. H. L. Zhang, Y. Du, P. V. Sushko, M. E. Bowden, V. Shutthanandan, S. Sallis, L. F. J. Piper, and S. A. Chambers, Hole-induced insulator-to-metal transition in $La_{1-x}Sr_xCrO_3$ epitaxial films, Phys. Rev. B **91**, 155129 (2015).

[7]S. Tao and J. T. S. Irvine, A redox-stable efficient anode for solid-oxide fuel cells, Nat. Mater. **2**, 320 (2003).

[8]K. A. Stoerzinger, Y. Du, K. Ihm, K. H. L. Zhang, J. Cai, J. T. Diulus, R. T. Frederick, G. S. Herman, E. J. Crumlin, and S. A. Chambers, Impact of Sr-incorporation on Cr oxidation and water dissociation in $La_{(1-x)}Sr_xCrO_3$, Adv. Mater. Interfaces **5**, 1701363 (2018).

[9]X. Marti, I. Fina, C. Frontera, J. Liu, P. Wadley, Q. He, R. J. Paull, J. D. Clarkson, J. Kudrnovský, I. Turek, J. Kuneš, D. Yi, J. H. Chu, C. T. Nelson, L. You, E. Arenholz, S. Salahuddin, J. Fontcuberta, T. Jungwirth, and R. Ramesh, Room-temperature antiferromagnetic memory resistor, Nat. Mater. **13**, 367 (2014).

[10]W. J. Hu, L. Hu, R. H. Wei, X. W. Tang, W. H. Song, J. M. Dai, X. B. Zhu, and Y. P. Sun, Nonvolatile resistive switching and physical mechanism in $LaCrO_3$ thin films, Chinese Phys. Lett. **35**, 047301 (2018).

[11]Y. Du, Li C, Zhang K H L, C. Li, K. H. L. Zhang, M. E. McBriarty, S. R. Spurgeon, H. S. Mehta, D. Wu, and S. A. Chambers, An all-perovskite pn junction based on transparent conducting p-$La_{1-x}Sr_xCrO_3$ epitaxial layers, Appl. Phys. Lett. **111**, 063501 (2017).

[12]R. Woods-Robinson, D. Broberg, A. Faghaninia, A. Jain, S. S. Dwaraknath, and K. A. Persson, Assessing High-throughput descriptors for prediction of transparent conductors, Chem. Mater. **30**, 8375 (2018).

[13]K. H. L. Zhang, K. Xi, M. G. Blamire, and R. G. Egdell, P-type transparent conducting oxides, J. Phys-Condens. Mat. **28**, 383002 (2016).

[14]S. A. Suvorov and A. P. Shevchik, A heating module equipped with lanthanum chromite-based heaters, Refract. Ind. Ceram+ **45**, 196 (2004).

[15]G. N. Greaves, A. L. Greer, R. S. Lakes, and T. Rouxel, Poisson's ratio and modern materials, Nat. Mater. **10**, 823 (2011).

[16]S. Ji, L. Li, H. B. Motra, F. Wuttke, S. Sun, K. Michibayashi, and M. H. Salisbury, J. Geophys. Poisson's ratio and auxetic properties of natural rocks, Res-Sol. Ea. **123**, 1161 (2018).

[17]C. W. Huang, W. Ren, V. C. Nguyen, Z. Chen, J. Wang, T. Sritharan, and L. Chen, Abnormal Poisson's ratio and linear compressibility in perovskite materials, Adv. Mater. **24**, 4170 (2012).

[18]Z. A. D. Lethbridge, R. I. Walton, A. S. H. Marmier, C. W. Smith, and K. E. Evans. Elastic anisotropy and extreme Poisson's ratios in single crystals, Acta Mater. **58**, 6444 (2010).

[19]*Materials fundamentals of molecular beam epitaxy*, edited by J. Y. Tsao (Academic Press, London, 1993).

[20]Z. Chen, Z. Luo, C. Huang, Y. Qi, P. Yang, L. You, C. Hu, T. Wu, J. Wang, C. Gao, T. Sritharan, and L. Chen, Low-symmetry monoclinic phases and polarization rotation path mediated by epitaxial strain in multiferroic $BiFeO_3$ thin films, Adv. Funct. Mater. **21**, 133 (2011).

[21]C. Adamo, X. Ke, H. Q. Wang, H. L. Xin, T. Heeg, M. E. Hawley, W. Zander, J. Schubert, P. Schiffer, D. A. Muller, L. Maritato, and D. G. Schlom, Effect of biaxial strain on the electrical and magnetic properties of (001) $La_{0.7}Sr_{0.3}MnO_3$ thin films, Appl. Phys. Lett. **95**, 112504 (2009).

[22]M. Choi, A. B. Posadas, C. A. Rodriguez, A. O'Hara, H. Seinige, A. J. Kellock, M. M. Frank, M. Tsoi, S. Zollner, V. Narayanan, and A. A. Demkov, Structural, optical, and electrical properties of strained La-doped $SrTiO_3$ films, J. Appl. Phys. **116**, 043705 (2014).

[23]G. Niu, J. Penuelas, L. Largeau, B. Vilquin, J. L. Maurice, C. Botella, G. Hollinger, and G. Saint-Girons, Evidence for the formation of two phases during the growth of $SrTiO_3$ on silicon, Phys. Rev. B **83**, 054105 (2011).

[24]D. G. Schlom, L. Chen, X. Pan, A. Schmehl, and M. A. Zurbuchen, A thin film approach to engineering functionality into oxides, J. Am. Ceram. Soc. **91**, 2429 (2008).

[25]D. Han, M. Bouras, C. Botella, A. Benamrouche, B. Canut, G. Grenet, G. Saint-Girons, and R. Bachelet, Structural properties of strained epitaxial $La_{1+\delta}CrO_3$ thin films, J. Vac. Sci. Technol. A **37**, 021512 (2019).

[26]G. Koster, B. L. Kropman, G. J. H. M. Rijnders, D. H. A. Blank, and H. Rogalla, Quasi-ideal strontium titanate crystal surfaces through formation of strontium hydroxide, Appl. Phys. Lett. **73**, 2920 (1998).

[27]The out-of-plane and in-plane epitaxial strain (ε_{zz} and ε_{xx}, respectively) due to the lattice mismatch $f = (a_{sub} - a_{film}) / a_{film}$ are defined here as: $\varepsilon_{zz} = (c_{film} - a_{bulk}) / a_{bulk}$ and $\varepsilon_{xx} = (a_{film} - a_{bulk}) / a_{bulk}$, where c_{film} and/or a_{film} is the measured out-of-plane/in-plane lattice parameter of the film, a_{bulk} the bulk lattice constant. The relaxation ratio R is defined here as $(a_{film} - a_{sub}) / (a_{bulk} - a_{sub})$, where a_{sub} is the in-plane parameter of corresponding substrate.

[28]R. Moalla, B. Vilquin, G. Saint-Girons, G. Sebald, N. Baboux, and R. Bachelet, Dramatic effect of thermal expansion mismatch on the structural, dielectric, ferroelectric and pyroelectric properties of low-cost epitaxial PZT films on $SrTiO_3$ and Si, CrystEngComm **18**, 1887 (2016).

[29]The thermal expansion coefficients at room temperature of LCO, LAO, LSAT, STO and DSO are 8.5×10^{-6} K^{-1}, 10×10^{-6} K^{-1}, 8.2×10^{-6} K^{-1}, 9×10^{-6} K^{-1}, and 8.4×10^{-6} K^{-1}, respectively.

[30]M. D. Scafetta, Z. Yang, S. R. Spurgeon, M. E. Bowden, T. C. Kaspar, S. M. Heald, and S. A. Chambers, Epitaxial growth and atomic arrangement in Fe_2CrO_4 on crystal symmetry matched (001) $MgAl_2O_4$, J. Vac. Sci. Technol. A **37**, 031511 (2019).

[31]L. Qiao, T. C. Droubay, M. E. Bowden, V. Shutthanandan, T. C. Kaspar, and S. A. Chambers, $LaCrO_3$ heteroepitaxy on $SrTiO_3$ (001) by molecular beam epitaxy, Appl. Phys. Lett. **99**, 061904 (2011)

[32]K. H. L. Zhang, P. V. Sushko, R. Colby, Y. Du, M. E. Bowden, and S. A. Chambers, Reversible nano-structuring of $SrCrO_{3-\delta}$ through oxidation and reduction at low temperature, Nat. Commun. **5**, 4669 (2014).

AIP Publishing

Journal of Applied Physics

ACCEPTED MANUSCRIPT

PLEASE CITE THIS ARTICLE AS DOI: 10.1063/1.5101049

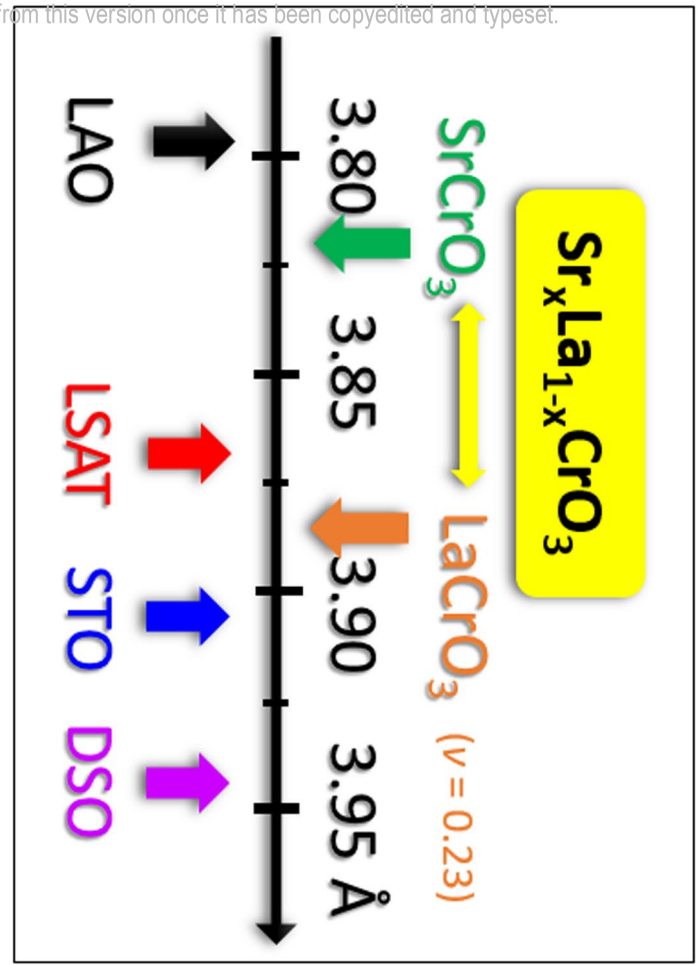

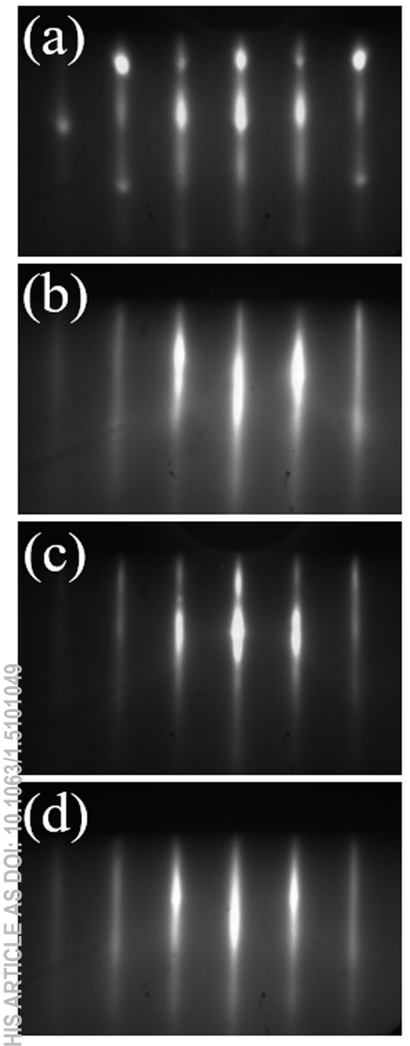

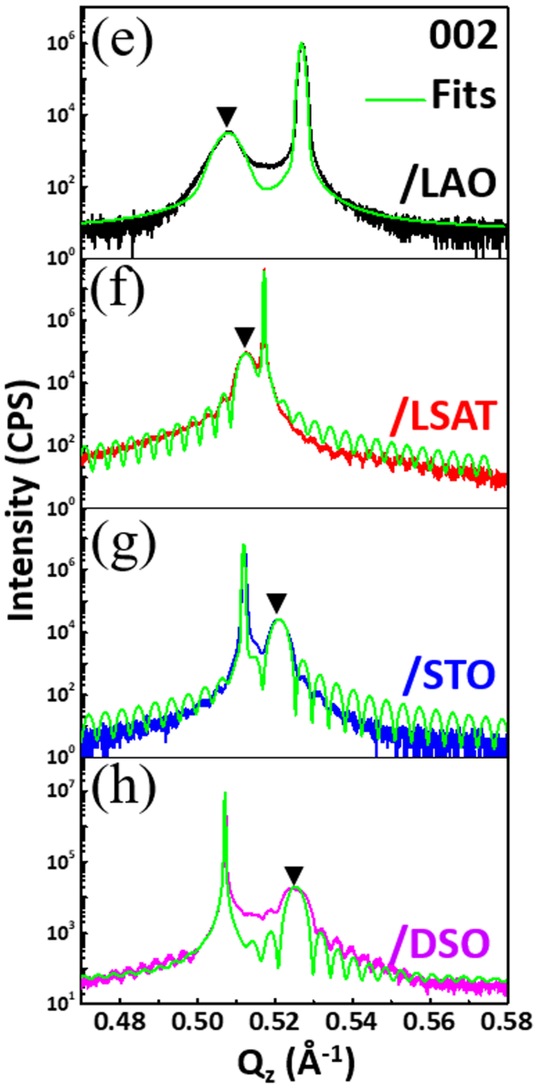

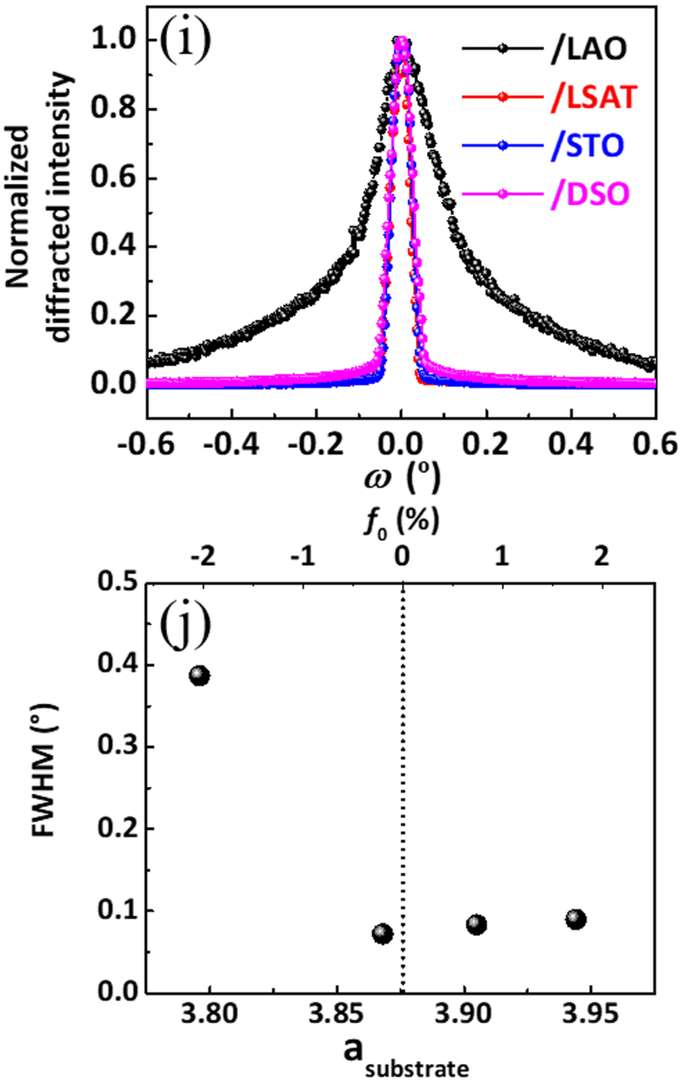

AIP Publishing

Journal of Applied Physics

PLEASE CITE THIS ARTICLE AS DOI: 10.1063/1.5101049

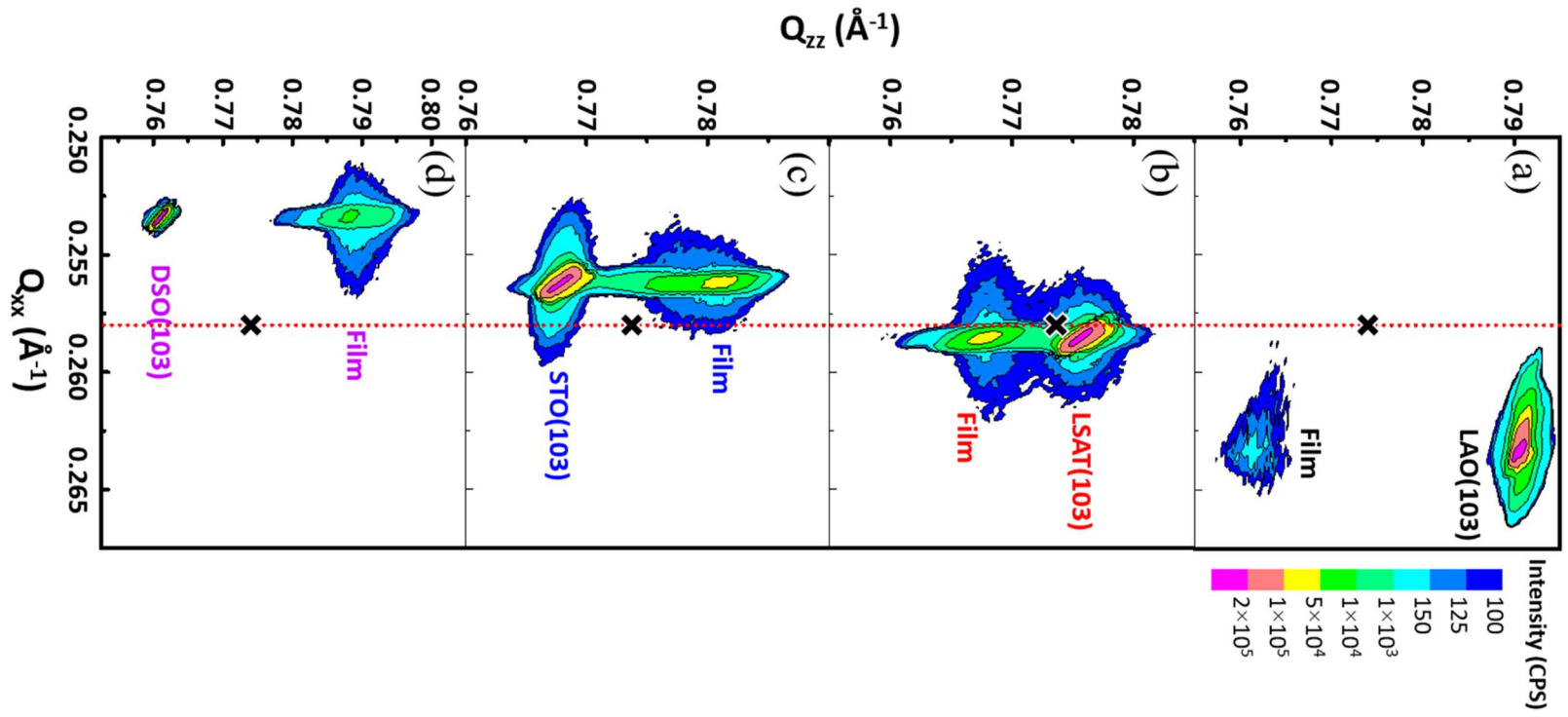

AIP Publishing

Journal of Applied Physics

ACCEPTED MANUSCRIPT

PLEASE CITE THIS ARTICLE AS DOI: 10.1063/1.5101049

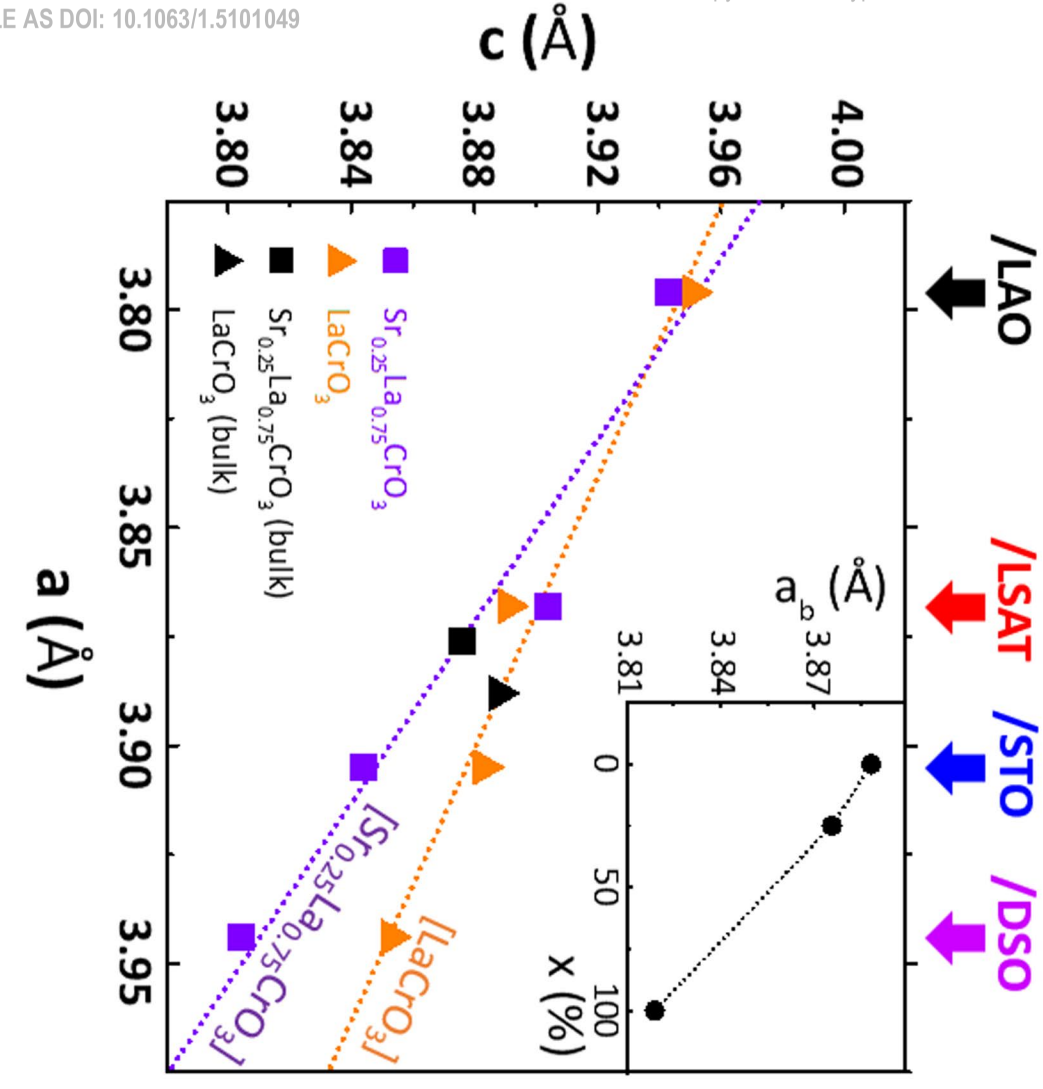

AIP Publishing

Journal of Applied Physics

ACCEPTED MANUSCRIPT

This is the author's peer reviewed, accepted manuscript. However, the online version of record will be different from this version once it has been copyedited and typeset.
PLEASE CITE THIS ARTICLE AS DOI: 10.1063/1.5101049